Spin-orbit-coupling-induced quantum droplet in ultracold Bose-Fermi mixtures

Xiaoling Cui
Beijing National Laboratory for Condensed Matter Physics, Institute of Physics, Chinese Academy of Sciences, Beijing 100190, People's Republic of China

(Received 15 April 2018; published 27 August 2018)

Quantum droplets have aroused much attention recently in view of their successful observations in ultracold homonuclear atoms. In this paper, we demonstrate an alternative mechanism for the formation of quantum droplets in heteronuclear atomic systems, i.e., by applying synthetic spin-orbit coupling (SOC). Taking the Bose-Fermi mixture, for example, we show that by imposing a Rashba SOC between the spin states of fermions such that all fermions occupy the lower helicity branch, the greatly suppressed Fermi pressure can enable the formation of Bose-Fermi droplets even for very weak boson-fermion attractions, which are insufficient to bound a droplet if without SOC. In such SOC-induced quantum droplets, the boson-fermion density ratio universally depends on the SOC strength, and they occur in the mean-field collapsing regime but with a negative fluctuation energy, distinct from the interaction-induced droplets found in literature. The accessibility of these Bose-Fermi droplets in ultracold Cs-Li and Rb-K mixtures is also discussed. Our results shed light on the droplet formation in a vast class of heteronuclear atomic systems through the manipulation of single-particle physics.

DOI: 10.1103/PhysRevA.98.023630

I. INTRODUCTION

Self-bound droplets are ubiquitous in nature, while their quantum mechanical analogs, quantum droplets, are challenging to achieve in physical systems as their appearance requires a sophisticated balance between attractive and repulsive forces. Recently, the study of quantum droplets has become a hot topic in the field of ultracold atoms. A pioneering work by Petrov showed that self-bound droplets of a two-component Bose gas can form in the mean-field collapsing regime [1], due to a balance between the mean-field attraction ($\sim -n^2$, n is the density) and Lee-Huang-Yang repulsion from quantum fluctuations ($\sim n^{5/2}$), and, importantly, they stay in the weak-coupling regime that can effectively avoid atom loss. To date, quantum droplets have been successfully observed in lanthanum atoms with a strong dipole-dipole interaction [2–5], and in alkali-metal boson mixtures [6–8] which exactly follow Petrov's scenario. Droplet formation has recently also been predicted in low-dimensional [9–12] and in photonic systems [13].

Given the successful explorations of quantum droplets in homonuclear systems [2–8], a question naturally arises as to whether such a peculiar state exists in heteronuclear systems, especially Bose-Fermi mixtures with coexisting different statistics. Actually, in this problem the Bose-Fermi and Bose-Bose mixtures share some similarities, in that the Fermi pressure in the former naturally plays the role of boson repulsion in the latter as a repulsive force, and both systems host an additional repulsion from quantum fluctuations [1,14]. So a Bose-Fermi droplet is expectable by fine tuning the boson-fermion attractions, as has been theoretically confirmed recently [15]. Nevertheless, one notes that the Fermi pressure scales as $\sim n^{5/3}$, which, compared to the boson repulsion ($\sim n^2$), generates a higher repulsive force in the dilute limit. Accordingly, a stronger attraction in Bose-Fermi mixtures is required to form a droplet. Strong interactions invalidate perturbative theory in treating the droplets, and inevitably induce severe atom losses in their realistic detection in experiments.

In this paper, we demonstrate a route to stabilize the quantum droplet, i.e., by introducing the spin-orbit coupling (SOC). In the past few years, cold-atom experiments have been successfully realized synthetic one-dimensional (1D) [16–26] and two-dimensional (2D) [27–29] types of SOC, and a highly symmetric SOC including the Rashba and isotropic types has also been theoretically proposed [30–36]. Our work is simply motivated by the fact that SOCs can significantly modify the single-particle physics in low-energy space. In particular, for a highly symmetric SOC, the resulting single-particle ground-state degeneracy in combination with interactions has been found to induce intriguing dimer [37–42], trimer [43–45], and many-body physics [46]. The effect of small SOC on droplets of homonuclear boson mixtures was studied in Ref. [47]. Here, we point out a robust mechanism in utilizing highly symmetric SOCs to drive the formation of stable three-dimensional (3D) Bose-Fermi droplets in a weak-coupling regime, which can be generalized to various heteronuclear atomic systems in different dimensions.

II. MODEL AND FORMALISM

To be concrete, we consider a Rashba spin-orbit-coupled Fermi gas, spin-selectively interacting with a Bose gas, which is described by the following Hamiltonian,

$$\begin{aligned} H = & \sum_{\mathbf{k}} \epsilon^b_{\mathbf{k}} b^\dagger_{\mathbf{k}} b_{\mathbf{k}} + \frac{U_{bb}}{V} \sum_{\mathbf{k},\mathbf{k}',\mathbf{Q}} b^\dagger_{\mathbf{k}} b^\dagger_{\mathbf{Q}-\mathbf{k}} b_{\mathbf{Q}-\mathbf{k}'} b_{\mathbf{k}'} \\ & + \sum_{\mathbf{k},\alpha} \epsilon^f_{\mathbf{k}} f^\dagger_{\mathbf{k},\alpha} f_{\mathbf{k},\alpha} \\ & + \frac{\lambda}{m_f} \sum_{\mathbf{k}} [(k_x - i k_y) f^\dagger_{\mathbf{k},\uparrow} f_{\mathbf{k},\downarrow} + \text{H.c.}] \\ & + \frac{U_{bf}}{V} \sum_{\mathbf{k},\mathbf{k}',\mathbf{Q}} f^\dagger_{\mathbf{k},\uparrow} b^\dagger_{\mathbf{Q}-\mathbf{k}} b_{\mathbf{Q}-\mathbf{k}'} f_{\mathbf{k}',\uparrow}. \end{aligned} \tag{1}$$

Here, $b^\dagger_{\mathbf{k}}$ and $f^\dagger_{\mathbf{k},\alpha}$ create a boson and a spin-α ($=\uparrow,\downarrow$) fermion, respectively, with energy $\epsilon^b_{\mathbf{k}} = \mathbf{k}^2/2m_b$ and $\epsilon^f_{\mathbf{k}} = \mathbf{k}^2/2m_f$; U_{bb} and U_{bf} are, respectively, the bare boson-boson and boson-fermion interactions, which can be related to scattering lengths a_{bb} and a_{bf} via renormalization equations, for instance, $1/U_{bf} = 1/g_{bf} - (1/V)\sum_{\mathbf{k}} 1/(2m_{bf}\mathbf{k}^2)$, with $g_{bf} = 2\pi a_{bf}/m_{bf}$, $m_{bf} = m_b m_f/(m_b+m_f)$, and V the volume. Here, we have neglected the background interaction between two-species fermions. Given a Rashba SOC with strength λ, the resulting single-fermion eigenenergy is $\epsilon^f_{\mathbf{k},\sigma} = [(k_\perp + \sigma\lambda)^2 + k_z^2]/(2m_f)$ (here, $k_\perp = \sqrt{k_x^2+k_y^2}$, $\sigma = \pm$ is the index of helicity branch), which gives a U(1) ground-state degeneracy in $\mathbf{k}$ space with $k_\perp = \lambda$. For brevity, we take $\hbar = 1$ throughout the paper.

In this work, we consider weakly interacting bosons with small a_{bb} (>0), and a weak attraction between the boson and spin-$\uparrow$ fermion with small a_{bf} (<0). Given the boson and fermion densities n_b and n_f, the energy density of the system can be written as

$$\mathcal{E}(n_b, n_f) = \mathcal{E}_b + \mathcal{E}_f + \mathcal{E}_{bf}, \tag{2}$$

where $\mathcal{E}_b = (2\pi a_{bb}/m_b)n_b^2[1 + (128/15\pi^{1/2})(n_b a_{bb}^3)^{1/2}]$ is the energy of a Bose gas with a Lee-Huang-Yang correction. $\mathcal{E}_f$ is the Fermi-sea energy under Rashba SOC,

$$\mathcal{E}_f = \frac{1}{V}\sum_{\mathbf{k},\sigma} \epsilon^f_{\mathbf{k},\sigma}\theta\big(E_f - \epsilon^f_{\mathbf{k},\sigma}\big), \tag{3}$$

with $E_f \equiv \lambda_f^2/(2m_f)$ the Fermi energy and λ_f the Fermi momentum, determined by the density constraint $n_f = \frac{1}{V}\sum_{\mathbf{k},\sigma}\theta(E_f - \epsilon^f_{\mathbf{k},\sigma})$. $\mathcal{E}_{bf} = \mathcal{E}^{(1)}_{bf} + \mathcal{E}^{(2)}_{bf}$ is the interaction energy between bosons and fermions, where $\mathcal{E}^{(1)}_{bf} = g_{bf} n_b n_{f,\uparrow}$ is the mean-field interaction energy, and $\mathcal{E}^{(2)}_{bf}$ ($\sim g_{bf}^2$) is the lowest-order correction due to density fluctuations, which can be obtained from the second-order perturbation theory as

$$\mathcal{E}^{(2)}_{bf} = n_b \frac{g_{bf}^2}{V}\sum_{\mathbf{k}}\Bigg(n_{f,\uparrow}\frac{2m_{bf}}{\mathbf{k}^2} - \frac{\epsilon^b_{\mathbf{k}}}{\omega_{\mathbf{k}}}\sum_{\mathbf{q},\sigma,\sigma'}\frac{1}{4V}\frac{\theta\big(E_f - \epsilon^f_{\mathbf{q},\sigma}\big)\theta\big(\epsilon^f_{\mathbf{k}+\mathbf{q},\sigma'} - E_f\big)}{\omega_k + \epsilon^f_{\mathbf{k}+\mathbf{q},\sigma'} - \epsilon^f_{\mathbf{q},\sigma}}\Bigg). \tag{4}$$

Here, $\omega_{\mathbf{k}} = \sqrt{\epsilon^b_{\mathbf{k}}(\epsilon^b_{\mathbf{k}} + 8\pi n_b a_{bb}/m_b)}$ is the Bogoliubov excitation energy of bosons. In the limit of $\lambda \to 0$, our result recovers the perturbative energy of Bose-Fermi mixtures without SOC [14]. Note that here we have neglected the phonon-mediated BCS ground-state energy of fermions, which is expected to be exponentially small in the weak-coupling limit [48].

Given $\mathcal{E}(n_b, n_f)$ in (2), one can obtain the chemical potentials $\mu_b = \partial\mathcal{E}/\partial n_b$, $\mu_f = \partial\mathcal{E}/\partial n_f$, and the pressure density $\mathcal{P} = \mathcal{P}_b + \mathcal{P}_f + \mathcal{P}_{bf}$, where

$$\mathcal{P}_b = n_b\frac{\partial\mathcal{E}_b}{\partial n_b} - \mathcal{E}_b, \quad \mathcal{P}_f = n_f\frac{\partial\mathcal{E}_f}{\partial n_f} - \mathcal{E}_f, \tag{5}$$

$$\mathcal{P}_{bf} = \mathcal{P}^{(1)}_{bf} + \mathcal{P}^{(2)}_{bf},$$

$$\mathcal{P}^{(i)}_{bf} = n_b\frac{\partial\mathcal{E}^{(i)}_{bf}}{\partial n_b} + n_f\frac{\partial\mathcal{E}^{(i)}_{bf}}{\partial n_f} - \mathcal{E}^{(i)}_{bf} \quad (i = 1, 2). \tag{6}$$

Here, $\mathcal{P}_b$ ($\mathcal{P}_f$) is the pressure caused by individual bosons (fermions), and $\mathcal{P}_{bf}$ is due to boson-fermion interactions and contributed from both the mean-field ($\mathcal{P}^{(1)}_{bf}$) and the quantum fluctuation ($\mathcal{P}^{(2)}_{bf}$) parts. The introduction of SOC will not change $\mathcal{P}_b$ and $\mathcal{P}^{(1)}_{bf}$, but will strongly modify $\mathcal{P}_f$ and $\mathcal{P}^{(2)}_{bf}$ as shown below.

Before proceeding, we should note that a stable ground-state droplet occurs when the following conditions are simultaneously satisfied:

$$\text{(i)}\quad \mathcal{E} < 0, \quad \mathcal{P} = 0,$$

$$\text{(ii)}\quad \mu_b\frac{\partial\mathcal{P}}{\partial n_f} = \mu_f\frac{\partial\mathcal{P}}{\partial n_b},$$

$$\text{(iii)}\quad \frac{\partial\mu_b}{\partial n_b} > 0, \quad \frac{\partial\mu_f}{\partial n_f} > 0, \quad \frac{\partial\mu_b}{\partial n_b}\frac{\partial\mu_f}{\partial n_f} > \left(\frac{\partial\mu_b}{\partial n_f}\right)^2,$$

where condition (i) describes a self-bound object that is in equilibrium with vacuum, a characteristic feature of a droplet [1]; condition (ii) further searches for the ground-state droplet with minimal energy [15], and (iii) ensures the droplet is stable against density fluctuations.

III. SPIN-ORBIT COUPLING INDUCED BOSE-FERMI DROPLETS

To gain the first insight on how a Rashba SOC affects the droplet formation, in Fig. 1 we take the ^{133}Cs-^{6}Li system and show its energy $\mathcal{E}$, pressure $\mathcal{P}$, and pressure components $\mathcal{P}_f$, $\mathcal{P}^{(2)}_{bf}$ as functions of SOC strength λ, for a given attraction $a_{bf} = -3a_{bb}$ and given densities $n_b a_{bb}^3 = 2\times10^{-5}$, $n_f a_{bb}^3 = 10^{-4}$. It can be seen that as λ increases from zero, both $\mathcal{E}$ and $\mathcal{P}$ decrease monotonically, such that at a critical $\lambda_c a_{bb} \sim 0.75$, $\mathcal{P}$ can reduce to zero with a negative $\mathcal{E}$, as marked by the red arrow in Fig. 1, which gives a droplet solution satisfying condition (i). During this process, $\mathcal{P}_f$ and $\mathcal{P}^{(2)}_{bf}$ also decrease, while the reduction of total $\mathcal{P}$ mainly comes from $\mathcal{P}_f$, since $\mathcal{P}^{(2)}_{bf}$ varies in a relatively smaller scale.

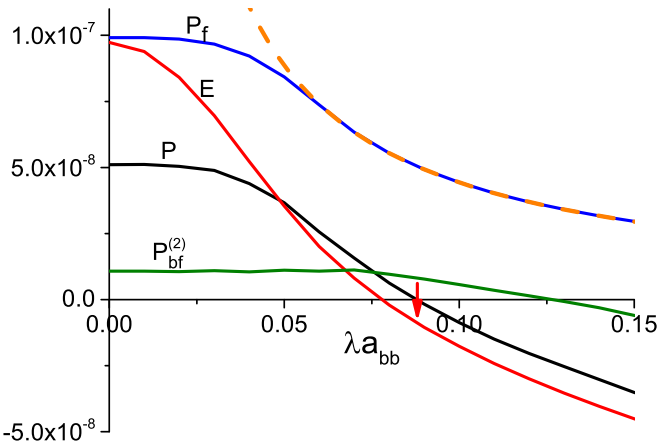

FIG. 1. $\mathcal{E}$, $\mathcal{P}$, $\mathcal{P}_f$, and $\mathcal{P}^{(2)}_{bf}$ [in units of $m_b a_{bb}^5/(2\pi V)$] as functions of λa_{bb}. Here, we take $n_b a_{bb}^3 = 2\times10^{-5}$, $n_f a_{bb}^3 = 10^{-4}$, $a_{bf} = -3a_{bb}$, and $m_b/m_f = 133/6$. The red arrow marks the location where the droplet condition (i) is satisfied. The orange dashed line shows a fit to $\mathcal{P}_f$ according to Eq. (7).

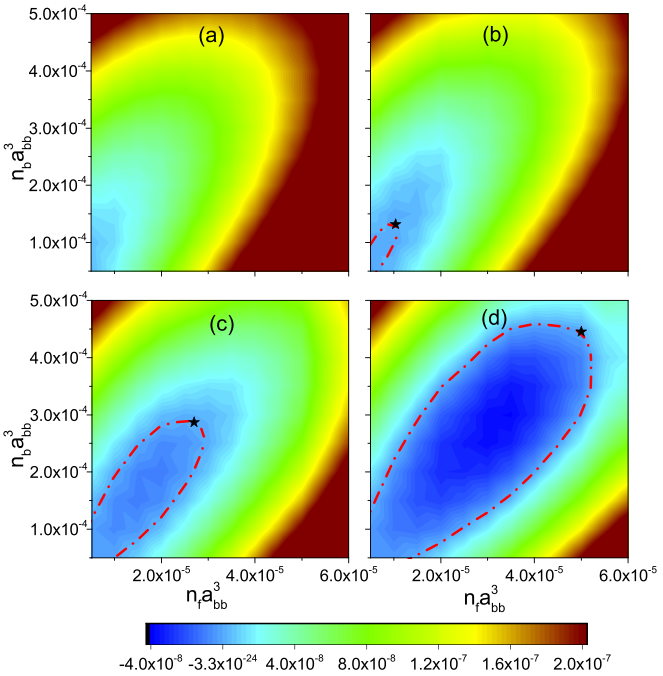

FIG. 2. Contour plots of $\mathcal{P}$ [in units of $m_b a_{bb}^5/(2\pi V)$] in the $(n_f a_{bb}^3, n_b a_{bb}^3)$ plane for different SOC strengths: (a) $\lambda a_{bb} = 0.02$, (b) 0.06, (c) 0.08, (d) 0.1. The red dashed-dotted lines in (b)–(d) denote zero-pressure loops, and the black stars mark the locations of ground-state droplets satisfying condition (ii). Here, we take $a_{bf} = -3a_{bb}$ and $m_b/m_f = 133/6$.

The suppressed Fermi pressure ($\mathcal{P}_f$) by Rashba SOC can be attributed to the U(1) ground-state degeneracy and thus the enhanced density of state $\rho(E)$ at low E, which approaches a constant ($\sim m_f\lambda$) as in an effective 2D geometry, rather than zero in the usual 3D case. As a result, in the presence of SOC, more fermions are accommodated in the low-E space, and this greatly suppresses $\mathcal{E}_f$ and $\mathcal{P}_f$. Specifically, in the low-density or strong-SOC regime where only the lower helicity branch is occupied, i.e., $n_f < n_{f,c} \equiv \lambda^3/4\pi$, we have

$$\mathcal{E}_f = \mathcal{P}_f = \frac{\pi}{\lambda m_f} n_f^2. \tag{7}$$

Therefore Rashba SOC can fundamentally alter the energy (pressure)-density scaling, from $\sim n_f^{5/3}$ in the usual case to $\sim n_f^2$, and this greatly suppresses $\mathcal{E}$ and $\mathcal{P}$ for a dilute Fermi gas. Moreover, Eq. (7) shows that $\mathcal{E}, \mathcal{P}$ can be further reduced by increasing SOC strength λ, as also shown in Fig. 1.

Given the robust single-particle physics modified by Rashba SOC, the suppression of $\mathcal{P}$ should generally apply to all boson-fermion densities. In Fig. 2, we show the contour plots of $\mathcal{P}(n_b, n_f)$ for a Cs-Li system taking a fixed $a_{bf} = -3a_{bb}$ and several different values of λa_{bb}. At $\lambda a_{bb} = 0.02$ [Fig. 2(a)], $\mathcal{P}$ is always positive, while it can be effectively reduced when increasing λa_{bb} to 0.06 [Fig. 2(b)], where it touches zero along a small loop in the (n_b, n_f) plane and becomes negative inside. By further increasing λa_{bb} to 0.08 and 0.1 [Figs. 2(c) and 2(d)], $\mathcal{P}$ is further reduced and the zero-pressure loop becomes even more enlarged. On each loop in Figs. 2(b)–2(d), the location of a ground-state droplet obeying condition (ii) is further marked by a star, and we have checked that all these solutions are with

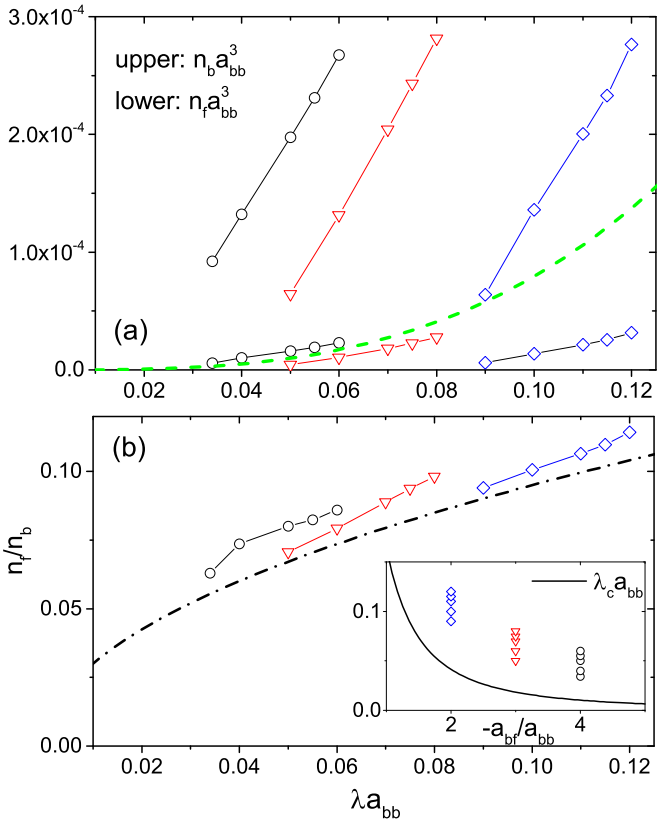

FIG. 3. (a) Boson and fermion densities and (b) their ratios as functions of λa_{bb} for the ground-state droplets at different scattering lengths $a_{bf}/a_{bb} = -4$ (black circles), -3 (red triangles), and -2 (blue diamonds). The green dashed line in (a) shows the critical fermion density $n_{f,c} = \lambda^3/(4\pi)$, below which only the lower helicity branch is occupied. In (b), the orange dashed-dotted line shows fits to Eq. (9); in the inset, the line shows a critical λ_c for mean-field collapse [see Eq. (8)], and the points shows actual λ for the data shown in the main plot. Here, $m_b/m_f = 133/6$.

$\mathcal{E} < 0$. In addition, because the stars all locate at the top right corner of the loops, we have $\partial\mathcal{P}/\partial n_b > 0$ and $\partial\mathcal{P}/\partial n_f > 0$, which automatically ensure the satisfaction of condition (iii). Therefore they represent stable ground-state droplets satisfying all conditions (i)–(iii).

Repeating the same procedure for different attraction strengths $a_{bf}/a_{bb} = -2$, -3, -4, we show in Fig. 3 the boson-fermion densities and their ratios as functions of λ for the ground-state Cs-Li droplets. As shown in Fig. 3(a), for $a_{bf} = -4a_{bb}$ (black circles), the droplets start to form at small $\lambda a_{bb} \sim 0.03$ with fermions occupying both the lower and upper helicity branches ($n_f > n_{f,c}$), thus these droplets are mainly interaction induced, similar to those without SOC [15]. Gradually reducing attraction to $a_{bf} = -3a_{bb}$ (red triangles), the droplets move to larger λ and n_f starts to drop below $n_{f,c}$. For a small attraction $a_{bf} = -2a_{bb}$ (blue diamonds), the droplet appears at $\lambda a_{bb} \gtrsim 0.09$ with $n_f \ll n_{f,c}$, i.e., the fermions are located near the bottom of the lower helicity branch with U(1) ground-state degeneracy. Such a droplet formation crucially relies on the suppressed Fermi pressure by Rashba SOC [see Eq. (7)], and can only appear for strong

SOC and weak attractions. Thus we call it the SOC-induced droplet, in order to distinguish from the interaction-induced ones at small or zero SOC. Below, we will extract several unique features for such kinds of droplets.

First, given Eq. (7), we see that SOC can conveniently tune the mean-field stability, and the collapse occurs at

$$\lambda > \lambda_c = \frac{8m_b m_f}{(m_b+m_f)^2}\frac{a_{bb}}{a_{bf}^2}. \tag{8}$$

The dependence of λ_c on a_{bf} is plotted in the inset of Fig. 3(b), and this qualitatively explains why a stronger SOC is required for droplet formation at weaker attractions, as shown in Fig. 3(a). Second, by requiring a minimal mean-field energy as in Bose-Bose mixtures [1], we obtain an optimal boson-fermion density ratio as

$$\left(\frac{n_f}{n_b}\right)_{\rm op} = \sqrt{\frac{2m_f}{m_b}}\sqrt{\lambda a_{bb}}. \tag{9}$$

This shows a universal dependence of the boson-fermion density ratio on the SOC strength, which is one of the characteristic features of the SOC-induced droplet. We see from Fig. 3(b) that Eq. (9) can well predict the actual density ratio for the SOC-induced droplets at $a_{bf} = -2a_{bb}$ (with a small discrepancy attributed to the quantum fluctuation effect), but deviates largely from that of the interaction-induced ones at a stronger attraction. Note that Eqs. (8) and (9) crucially rely on the energy relation (7) for large λ [$>(4\pi n_f)^{1/3}$], which cannot be extended to the zero λ limit.

The SOC-induced droplets also significantly differ from the interaction-induced ones in quantum fluctuations. To compare the fluctuation effects for all sets of parameters, we investigate the relative fluctuation energy and pressure, denoted by $R_E \equiv \mathcal{E}_{bf}^{(2)}/|\mathcal{E}_{bf}^{(1)}|$ and $R_P \equiv \mathcal{P}_{bf}^{(2)}/|\mathcal{P}_{bf}^{(1)}|$, respectively. In Fig. 4, we plot R_E, R_P and the total energy $\mathcal{E}$ for the droplet solutions in Fig. 3. One can see that at given a_{bf}, $\mathcal{E}$ monotonically

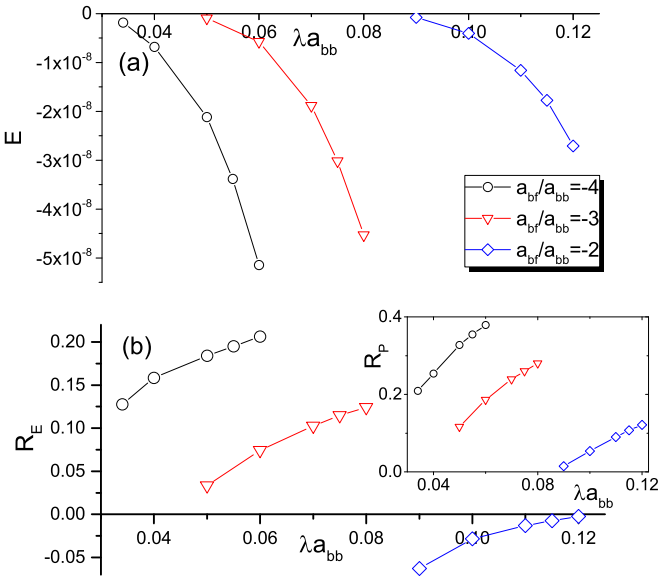

FIG. 4. (a) Energy density $\mathcal{E}$ [in units of $m_b a_{bb}^5/(2\pi V)$] and (b) the relative fluctuation energy (pressure) R_E (R_P) as functions of λ for the droplet solutions in Fig. 3.

decreases as λ increases. For the same window of $|\mathcal{E}| \in [2\times 10^{-9}, 3\times 10^{-8}]$, R_E and R_P can range within [12%, 20%] and [20%, 35%] for $a_{bf} = -4a_{bb}$; the numbers continuously decrease for a weaker attraction, and finally for the SOC-induced droplet at $a_{bf} = -2a_{bb}$, R_E turns negative, and $|R_E|$ and R_P can be very small ($|R_E| < 5\%$, $R_P < 12\%$).

Three remarks are in order. First, the reason that the SOC-induced droplets host very small $|R_E|$ and R_P can be attributed to their appearance in the weak-coupling regime, i.e., small a_{bf}, which guarantees the validity of the perturbative treatment in theory as well as the practical stability in experiments. In comparison, the interaction-induced Bose-Fermi droplets have a much higher R_E [49]. Second, the SOC-induced droplets can exhibit a negative fluctuation energy $\mathcal{E}_{bf}^{(2)} < 0$, which is very rare in 3D systems. This is, again, associated with the enhanced density of states by Rashba SOC, such that the low-energy particle-hole excitations are more activated and the second term in Eq. (4) can dominate to produce a negative $\mathcal{E}_{bf}^{(2)}$. A similar effect by a Rashba SOC has been shown to enhance the quantum depletion of a 3D Bose condensate [50,51]. Third, despite $\mathcal{E}_{bf}^{(2)} < 0$, the fluctuation pressure $\mathcal{P}_{bf}^{(2)}$ is still positive given $\partial\mathcal{E}_{bf}^{(2)}/\partial n_{b,f} > 0$. Therefore such a droplet is stabilized in the mean-field collapsing regime by the fluctuation pressure, rather than the fluctuation energy. This is to be contrasted with the droplets studied in the literature [1,9–12,15] where fluctuation energy and pressure share the same sign.

Now we discuss the accessibility of SOC-induced droplets in ultracold Bose-Fermi mixtures [52], such as the ^{133}Cs-^{6}Li and ^{87}Rb-^{40}K mixtures. For a laser-generated SOC, typically the maximum λ is given by the laser wave vector, i.e., $\lambda_{\rm max} \sim 2\pi/1000\ {\rm nm}^{-1}$. For a Cs-Li system near 892-G Feshbach resonance [53], the Cs-Cs scattering length $a_{bb} \sim 15$ nm, giving $\lambda_{\rm max} a_{bb} \sim 0.1$. According to Fig. 3, a Cs-Li droplet can form at $a_{bf} = -2a_{bb} = -30$ nm, with densities $n_f = 0.1 n_b = 4\times 10^{12}\ {\rm cm}^{-3}$. For a Rb-K system near 546-G resonance [54], given a smaller Rb-Rb scattering length $a_{bb} \sim 5$ nm, we have $\lambda_{\rm max} a_{bb} \sim 0.033$. According to Eqs. (8) and (9), the minimum attraction required for mean-field collapse is $a_{bf} \sim -7.6a_{bb} \sim 40$ nm, and the optimal density ratio in the droplet is $n_f/n_b \sim 0.17$. We note that in both Cs-Li and Rb-K droplets, $n_b \gg n_f$, similar to the Bose polaron system as has been realized in cold atoms without SOC [54–56].

IV. SUMMARY AND OUTLOOK

To summarize, our work shows that aside from fine-tuning interactions, SOC can be used as an independent and efficient tool for generating quantum droplets. Due to the distinct driving force, the SOC-induced droplets exhibit a number of unique features as compared to the interaction-induced droplets, such as a required much weaker-coupling strength, a universal density ratio, and an opposite sign of energy and pressure due to quantum fluctuations. Our results have direct relevance to the cold atomic gases of Cs-Li and Rb-K mixtures.

The SOC-induced droplet has a number of implications as shown below. First, it offers an ideal platform to study the topological edge states when further combining SOC with interactions, since the droplet configuration naturally provides a surface or boundary for cold atoms without resorting to external potentials. Moreover, this work offers a possibility

to engineer quantum droplets by changing the single-particle physics, which liberates the droplet from a strong interaction and thus helps to avoid atom loss in practical cold-atom experiments. The associated mechanism can be generalized to a vast class of heteronuclear atomic systems in various geometries. In particular, this work sheds light on the droplet formation even in Fermi-Fermi mixtures and in mixed dimensions.

ACKNOWLEDGMENTS

We thank D. Petrov for stimulating discussions on droplets. This work is supported by the National Key Research and Development Program of China (No. 2018YFA0307600, No. 2016YFA0300603), and the National Natural Science Foundation of China (No. 11622436, No. 11421092, and No. 11534014).

[1] D. S. Petrov, Phys. Rev. Lett. **115**, 155302 (2015).

[2] I. Ferrier-Barbut, H. Kadau, M. Schmitt, M. Wenzel, and T. Pfau, Phys. Rev. Lett. **116**, 215301 (2016).

[3] M. Schmitt, M. Wenzel, B. Böttcher, I. Ferrier-Barbut, and T. Pfau, Nature (London) **539**, 259 (2016).

[4] I. Ferrier-Barbut, M. Schmitt, M. Wenzel, H. Kadau, and T. Pfau, J. Phys. B **49**, 214004 (2016).

[5] L. Chomaz, S. Baier, D. Petter, M. J. Mark, F. Wächtler, L. Santos, and F. Ferlaino, Phys. Rev. X **6**, 041039 (2016).

[6] C. R. Cabrera, L. Tanzi, J. Sanz, B. Naylor, P. Thomas, P. Cheiney, and L. Tarruell, Science **359**, 301 (2018).

[7] P. Cheiney, C. R. Cabrera, J. Sanz, B. Naylor, L. Tanzi, and L. Tarruell, Phys. Rev. Lett. **120**, 135301 (2018).

[8] G. Semeghini, G. Ferioli, L. Masi, C. Mazzinghi, L. Wolswijk, F. Minardi, M. Modugno, G. Modugno, M. Inguscio, and M. Fattori, Phys. Rev. Lett. **120**, 235301 (2018).

[9] D. S. Petrov and G. Astrakharchik, Phys. Rev. Lett. **117**, 100401 (2016).

[10] D. Edler, C. Mishra, F. Wächtler, R. Nath, S. Sinha, and L. Santos, Phys. Rev. Lett. **119**, 050403 (2017).

[11] Y. Sekino and Y. Nishida, Phys. Rev. A **97**, 011602(R) (2018).

[12] A. Pricoupenko and D. S. Petrov, Phys. Rev. A **97**, 063616 (2018).

[13] N. Westerberg, K. E. Wilson, C. W. Duncan, D. Faccio, E. M. Wright, P. Öhberg, and M. Valiente, arXiv:1801.08539.

[14] L. Viverit and S. Giorgini, Phys. Rev. A **66**, 063604 (2002).

[15] T. Karpiuk, D. Rakshit, M. Brewczyk, and M. Gajda, arXiv:1801.00346.

[16] Y.-J. Lin, K. Jiménez-García, and I. B. Spielman, Nature (London) **471**, 83 (2011).

[17] Y.-J. Lin, R. L. Compton, K. Jiménez-Garcia, W. D. Phillips, J. V. Porto, and I. B. Spielman, Nat. Phys. **7**, 531 (2011).

[18] J.-Y. Zhang, S.-C. Ji, Z. Chen, L. Zhang, Z.-D. Du, B. Yan, G.-S. Pan, B. Zhao, Y.-J. Deng, H. Zhai, S. Chen, and J.-W. Pan, Phys. Rev. Lett. **109**, 115301 (2012).

[19] R. A. Williams, L. J. LeBlanc, K. Jiménez-Garci, M. C. Beeler, A. R. Perry, W. D. Phillips, and I. B. Spielman, Science **335**, 314 (2012).

[20] P. Wang, Z.-Q. Yu, Z. Fu, J. Miao, L. Huang, S. Chai, H. Zhai, and J. Zhang, Phys. Rev. Lett. **109**, 095301 (2012).

[21] L. W. Cheuk, A. T. Sommer, Z. Hadzibabic, T. Yefsah, W. S. Bakr, and M. W. Zwierlein, Phys. Rev. Lett. **109**, 095302 (2012).

[22] C. Qu, C. Hamner, M. Gong, C. Zhang, and P. Engels, Phys. Rev. A **88**, 021604(R) (2013).

[23] M. C. Beeler, R. A. Williams, K. Jiménez-Garcia, L. J. LeBlanc, A. R. Perry, and I. B. Spielman, Nature (London) **498**, 201 (2013).

[24] J.-Y Zhang, S.-C. Ji, L. Zhang, Z.-D. Du, W. Zheng, Y.-J. Deng, H. Zhai, S. Chen, and J.-W. Pan, Nat. Phys. **10**, 314 (2014).

[25] R. A. Williams, M. C. Beeler, L. J. LeBlanc, K. Jimenez-Garcia, and I. B. Spielman, Phys. Rev. Lett. **111**, 095301 (2013)

[26] Z. Fu, L. Huang, Z. Meng, P. Wang, L. Zhang, S. Zhang, H. Zhai, P. Zhang, and J. Zhang, Nat. Phys. **10**, 110 (2014).

[27] L. Huang, Z. Meng, P. Wang, P. Peng, S.-L. Zhang, L. Chen, D. Li, Q. Zhou, and J. Zhang, Nat. Phys. **12**, 540 (2016).

[28] Z. Meng, L. Huang, P. Peng, D. Li, L. Chen, Y. Xu, C. Zhang, P. Wang, and J. Zhang, Phys. Rev. Lett. **117**, 235304 (2016).

[29] Z. Wu, L. Zhang, W. Sun, X.-T. Xu, B.-Z. Wang, S.-C. Ji, Y. Deng, S. Chen, X.-J. Liu, and J.-W. Pan, Science **354**, 83 (2016).

[30] D. L. Campbell, G. Juzeliūnas, and I. B. Spielman, Phys. Rev. A **84**, 025602 (2011).

[31] J. D. Sau, R. Sensarma, S. Powell, I. B. Spielman, and S. Das Sarma, Phys. Rev. B **83**, 140510(R) (2011).

[32] Z. F. Xu and L. You, Phys. Rev. A **85**, 043605 (2012).

[33] X.-J. Liu, K. T. Law, and T. K. Ng, Phys. Rev. Lett. **112**, 086401 (2014).

[34] B. M. Anderson, I. B. Spielman, and G. Juzeliūnas, Phys. Rev. Lett. **111**, 125301 (2013).

[35] Z.-F. Xu, L. You, and M. Ueda, Phys. Rev. A **87**, 063634 (2013)

[36] B. M. Anderson, G. Juzeliūnas, V. M. Galitski, and I. B. Spielman, Phys. Rev. Lett. **108**, 235301 (2012).

[37] J. P. Vyasanakere and V. B. Shenoy, Phys. Rev. B **83**, 094515 (2011).

[38] X. Cui, Phys. Rev. A **85**, 022705 (2012).

[39] P. Zhang, L. Zhang, and W. Zhang, Phys. Rev. A **86**, 042707 (2012).

[40] Y. Wu and Z. Yu, Phys. Rev. A **87**, 032703 (2013).

[41] S.-J. Wang and C. H. Greene, Phys. Rev. A **91**, 022706 (2015).

[42] Q. Guan and D. Blume, Phys. Rev. A **94**, 022706 (2016).

[43] Z. Y. Shi, X. Cui, and H. Zhai, Phys. Rev. Lett. **112**, 013201 (2014).

[44] Z. Y. Shi, H. Zhai, and X. Cui, Phys. Rev. A **91**, 023618 (2015).

[45] X. Cui and W. Yi, Phys. Rev. X **4**, 031026 (2014).

[46] See reviews: H. Zhai, Int. J. Mod. Phys. B **26**, 1230001 (2012); Rep. Prog. Phys. **78**, 026001 (2015); V. Galitski and I. B. Spielman, Nature (London) **494**, 49 (2013); N. Goldman, G. Juzeliūnas, P. Öhberg, and I. B. Spielman, Rep. Prog. Phys. **77**, 126401 (2014); X. Zhou, Y. Li, Z. Cai, and C. Wu, J. Phys. B: At. Mol. Opt. Phys. **46**, 134001 (2013); W. Yi, W. Zhang, and X. Cui, Sci. China: Phys., Mech. Astron. **58**, 1 (2015).

[47] Y. Li, Z. Luo, Y. Liu, Z. Chen, C. Huang, S. Fu, H. Tan, and B. A. Malomed, New J. Phys. **19**, 113043 (2017).

[48] The phonon-mediated fermion-fermion coupling strength scales as $\sim g_{bf}^2$ [see, for instance, L. Viverit, C. J. Pethick, and

H. Smith, Phys. Rev. A **61**, 053605 (2000)]. With a Rashba SOC, the low-E space is 2D-like and such a weak interaction leads to an exponentially shallow two-body bound state with $E_{2b} \sim e^{-c/(\lambda g_{bf}^2)}$ [37]. For the BCS ground state of a many-body system, this lead to an exponentially small condensation energy $E_{\rm BCS} = -\rho\Delta^2/2 \propto -E_{2b}$ [here, we have used the (effective) 2D pairing gap $\Delta \propto E_{2b}$].

[49] We note that the minimal R_E can be as large as 27% for Cs-Li droplets without SOC [15].

[50] T. Ozawa and G. Baym, Phys. Rev. Lett. **109**, 025301 (2012).

[51] X. Cui and Q. Zhou, Phys. Rev. A **87**, 031604(R) (2013).

[52] See a recent review paper on Bose-Fermi mixtures in cold atoms, by R. Onofrio, Phys. Usp. **59**, 1129 (2016).

[53] B. J. DeSalvo, K. Patel, J. Johansen, and C. Chin, Phys. Rev. Lett. **119**, 233401 (2017).

[54] M.-G. Hu, M. J. Van de Graaff, D. Kedar, J. P. Corson, E. A. Cornell, and D. S. Jin, Phys. Rev. Lett. **117**, 055301 (2016).

[55] N. B. Jorgensen, L. Wacker, K. T. Skalmstang, M. M. Parish, J. Levinsen, R. S. Christensen, G. M. Bruun, and J. J. Arlt, Phys. Rev. Lett. **117**, 055302 (2016).

[56] F. Schmidt, D. Mayer, Q. Bouton, D. Adam, T. Lausch, N. Spethmann, and A. Widera, arXiv:1802.08702.